Smart Structures and Systems, *Vol. 21, No. 4 (2018) 479-491*
DOI: https://doi.org/10.12989/sss.2018.21.4.479

Seismic behavior of properly designed CBFs equipped with NiTi SMA braces

Canxing Qiu*, Yichen Zhang[a], Jian Qi[b] and Han Li[c]

School of civil engineering, Shandong University, Jinan 250061, Shandong, China

(Received December 30, 2017, Revised February 6, 2018, Accepted February 28, 2018)

Abstract. Shape memory alloys (SMA) exhibit superelasticity which refers to the capability of entirely recovering large deformation upon removal of applied forces and dissipating input energy during the cyclic loading reversals when the environment is above the austenite finish temperature. This property is increasingly favored by the earthquake engineering community, which is currently developing resilient structures with prompt recovery and affordable repair cost after earthquakes. Compared with the other SMAs, NiTi SMAs are widely deemed as the most promising candidate in earthquake engineering. This paper contributes to evaluate the seismic performance of properly designed concentrically braced frames (CBFs) equipped with NiTi SMA braces under earthquake ground motions corresponding to frequently-occurred, design-basis and maximum-considered earthquakes. An *ad hoc* seismic design approach that was previously developed for structures with idealized SMAs was introduced to size the building members, by explicitly considering the strain hardening characteristics of NiTi SMA particularly. The design procedure was conducted to compliant with a suite of ground motions associated with the hazard level of design-basis earthquake. A total of four six-story CBFs were designed by setting different ductility demands for SMA braces while designating with a same interstory drift target for the structural systems. The analytical results show that all the designed frames successfully met the prescribed seismic performance objectives, including targeted maximum interstory drift, uniform deformation demand over building height, eliminated residual deformation, controlled floor acceleration, and slight damage in the main frame. In addition, this study indicates that the strain hardening behavior does not necessarily impose undesirable impact on the global seismic performance of CBFs with SMA braces.

Keywords: seismic performance; NiTi, shape memory alloy; concentrically braced frame

1. Introduction

Superelastic SMAs are a class of metal alloys, which have gained increasing interests in the field of seismic applications over past years, attributed to the capability of ideally recovering large deformation and meanwhile absorbing input energy (Hadi and Akbari 2016, Park and Park 2016, Ozbulut *et al.* 2011, Song *et al.* 2006, Zhang and Zhu 2007), when the ambient temperature is above the austenite finish temperature threshold. Such metal alloys have high diversity due to the variety in the metal components, people have evaluated the potential of many types of SMAs in seismic applications, primarily including NiTi (DesRoches *et al.* 2004, Dolce *et al.* 2000, Liu *et al.* 2011, Fang *et al.* 2017, Gao *et al.* 2016, Qian *et al.* 2016), polycrystalline CuAlBe (Zhang *et al.* 2010), monocrystalline CuAlBe (Qiu and Zhu 2014), CuAlMn (Araki *et al.* 2011), and FeNiCuAlTaB (Dezfuli and Alam 2013). Compared to the other types of SMAs, NiTi SMAs are particularly favored by the community of earthquake engineering, because of relatively low cost, excellent corrosion resistance, high fatigue life, large elastic strain, and good damping behavior (DesRoches and Smith 2004). Fatigue effects of SMA are critical to seismic applications. Sufficient fatigue life for SMAs is necessary for successfully enduring repeated earthquake induced strain cycles. Fortunately, the high fatigue life makes NiTi SMAs promising material for being the seismically resistant components (Carreras *et al.* 2011, Casciati and Marzi 2010, 2011, Torra *et al.* 2014, Casciati *et al.* 2017).

Among many applications of NiTi SMAs exploited in different forms (Casciati and Faravelli 2009, Fang *et al.* 2014, Ozbulut *et al.* 2011, Shrestha and Hao 2016, Song *et al.* 2006, Torra *et al.* 2014, Ozbulut and Silwal 2016), a group of studies focused on exploring the NiTi SMAs as the kernel component of high-performance braces installed in concentrically braced frames (CBFs) (Abou-Elfath 2017, McCormick *et al.* 2007, Moradi *et al.* 2014, Qiu and Zhu 2017a). CBFs constitute a substantial portion of existing structural system in earthquake-prone regions, while people have noticed several major challenges associated with existing braces, which include the conventional braces and buckling-restrained braces (BRB). The conventional braces suffer from buckling-induced instability and consequently loss sustaining capacity upon compression (Fahnestock *et al.* 2007), and BRBs tend to accumulate excessive residual deformation after earthquakes, albeit their high damping capacity effectively controls peak seismic demands for frames (Sabelli *et al.* 2003). To address above problems, people found a potential solution by inventing high

*Corresponding author, Assistant Professor
E-mail: qiucanxing@sdu.edu.cn
[a] M.S. Student
[b] M.S. Student
[c] M.S. Student

ISSN: 1738-1584 (Print), 1738-1991 (Online)

performance braces based on NiTi SMA wires, i.e., NiTi SMA brace. Supported by the MENSIDE project, Dolce *et al.* (2010) manufactured large-scale SMA braces and validated the seismic performance within reinforced concrete frame through shake table tests. Later, Qiu and Zhu (2017b) further assessed the dynamic behavior of SMA braces within steel frames by subjecting the testing model to a series of far- and near- fault earthquake ground motions, and observed desirable performance. Besides with scaled-model tests, numerical analyses further revealed salient benefits of SMA braces with respect to their seismic behavior, through comparisons with the other representative braces. For example, McCormick *et al.* (2007) numerically compared steel braces with SMA braces, and indicated the later one performed better by producing smaller peak and residual deformation. Moradi *et al.* (2014) conducted incremental dynamic analysis, and illustrated that the CBFs using SMA braces exhibited more uniform distribution of inelastic response over the building height as compared with the responses of BRBFs. Zhu and Zhang (2008) showed SMA braces are superior to BRBs in controlling residual deformation for CBFs. Qiu and Zhu (2016) found higher-mode effect is more pronounced in CBFs with SMA braces than that with BRBs. Qiu *et al.* (2018) highlighted that the failure probabilities of CBFs with SMA braces are lower than that with BRBs, provided the residual deformation is considered.

It is worth noting that the SMA braces installed in the CBFs were somewhat artificially designed in past comparative studies, primarily because SMAs, as an emerging material in civil engineering, are yet to be included in current design codes. Usually, the design philosophy for SMA braces is to calibrate the their strength capacity equivalent to that of existing braces (Abou-Elfath 2017, McCormick *et al.* 2007), or to adjust the elastic properties of SMA braces by iterations until arrive at a desirable behavior (Zhu and Zhang 2008). Similar treatment is also adopted to design the other types of SMA-based devices (Andrawes and DesRoches 2005). Later, Qiu and Zhu (2017a) developed of an *ad hoc* design method for CBFs with SMA braces, and examined the generality on various SMA braces (Hou *et al.* 2017) and different frames (Qiu *et al.* 2017). Therefore, this makes it viable to design SMA braces with targeted capacities in a more reasonable manner and to mobilize the focus on the seismic behavior of SMA braces. In this paper, the research aim is concentrated on the seismic characteristics of CBFs equipped with SMA braces, and to particularly discuss the outcomes when different performance targets are prescribed in the design procedure.

2. NiTi SMA braces

In formal applications, SMA wires should have stable hysteretic properties. To this end, the applied wires should be properly trained by subjecting them to sufficient strain cycles prior to formal using, with the aims to eliminate the thermal effect and creep problem. In this study, the SMA wires were subjected to twenty loading cycles of 8% strain, as shown in Fig. 1(a). It is seen that the hysteretic properties of SMA wires gradually stabilized after being trained. In other words, the thermal effect and creep problem are well eliminated. Fig. 1(b) shows the stress-strain relationships of the trained SMA wires, corresponding to strains of 1% to 8% with an increment of 1%. Fig. 1(b) presents the testing result of the 1.0 mm diameter NiTi SMA wire upon a loading rate of 1.0 Hz at room temperature (Qiu and Zhu 2014). The salient mechanical property is essentially characterized by the recoverable phase transformation between austenite and martensite alignments of crystals. The forward phase transformation of SMA is analogous to the yielding behavior of steel, thus 'yielding' is also used to describe this behavior. The elastic modulus of austenite phase, E_A, is about 50 GPa. The forward phase transformation is activated at a strain of 1.0%, i.e., ε_{Ms} = 1.0%, by a stress level of approximately 500 MPa, i.e., σ_{Ms} = 500 MPa, and then followed by a phase transformation process, leading to a stable 'yielding' plateau. At a strain, ε_{Mf}, of 6.0%, the forward phase transformation is completed and the alloy is entirely transformed into martensite phase with a modulus of approximately 15 GPa, i.e. E_M = 15 GPa. The suddenly increased stress level is thus denoted as the strain hardening behavior. Seismic loads usually generate several large strain cycles in the material, so the fracture level of SMA should be higher than the largest strain demand caused by earthquakes. Regarding the number of working cycles, it should be sufficiently large to endure the seismic loads. According to a prior study (Hou *et al.* 2017), for different SMAs, various design targets should be properly defined, depending on the material properties. In terms of currently selected NiTi SMA wires, the fracture level and fatigue life were reported high enough for seismic applications (Qiu and Zhu 2014).

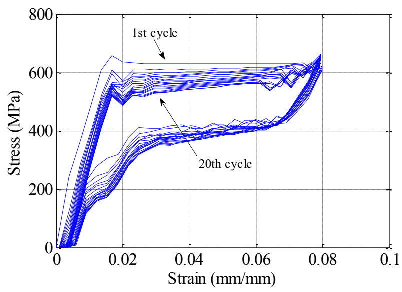

(a) training treatment

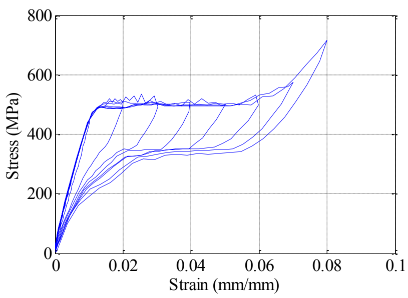

(b) stress-strain relationships of the trained wire (data are extracted from reference (Qiu and Zhu 2014))

Fig. 1 Cyclic behavior of 1.0 mm diameter NiTi SMA wire upon a loading rate of 1.0 Hz at room temperature

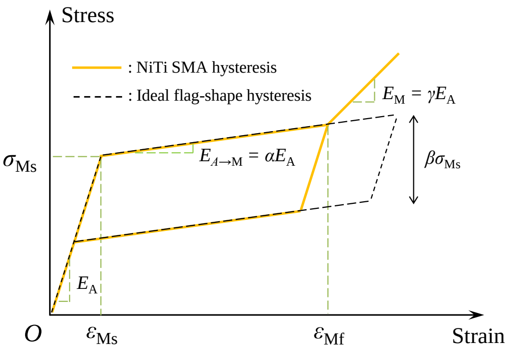

Fig. 2 Simplified NiTi SMA hysteresis and idealized flag-shape hysteresis

Two additional parameters, α and β, are introduced to measure the 'post-yielding' stiffness ratio and hysteresis width, respectively. All the referred parameters are shown in Fig. 2. For the current NiTi SMA wire, the values of α, β and γ are measured to be approximately 0.01, 0.5 and 0.3, respectively. For the simplified hysteresis of NiTi SMA, it neglects the cyclic-effect induced property degradation and strain-hardening induced residual deformation, which were found have little effect on the seismic responses of structures equipped with SMA-based components (Andrawes and DesRoches 2008). Also shown in Fig. 2 is the comparison between simplified NiTi SMA hysteresis and idealized flag-shape hysteresis. Compared with the idealized one, the NiTi SMA hysteresis explicitly includes the strain hardening behavior, which is probably activated by severe earthquakes. Thus, it is necessary to take into account this effect, with the aim to better observe the seismic behavior of CBFs equipped with SMA braces.

It is noted that the currently considered SMA wires belong to thinner types. As reported by the study (Qiu and Zhu 2017b), the targeted strength of the SMA braces was actually achieved by using bundles of wires to fulfill the capacity demand of the testing frame model, instead of using thick wires. In real applications, hundreds of wires are required to work in parallel for sustaining seismic forces, and the final braces will be able to maintain the flag-shaped hysteretic properties of a single wire. However, if thicker wires are adopted, the hysteretic curves would be S-shaped cycle (Torra *et al.* 2017), and the idealized hysteretic behavior would be no longer flag-shaped cycle. Further, more work is needed to discuss the effect of hysteretic properties in future.

(a) actual device

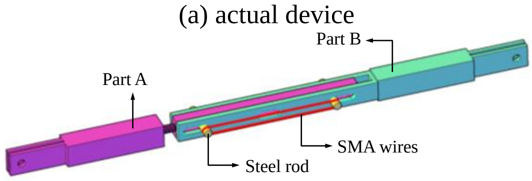

(b) schematic configuration

Fig. 3 NiTi SMA brace (Qiu and Zhu 2017b)

Fig. 3 shows a viable configuration of NiTi SMA brace. The brace was fabricated at an in-house laboratory, as shown in Fig. 3(a), and the seismic capacity has been successfully validated by dynamic tests within a reduced-scale steel frame on shake table (Qiu and Zhu 2017b). The core of the device is the NiTi SMA wires, which are always stretched through the mechanism illustrated in Fig. 3(b), regardless of the device being tensioned or compressed. Parts A and B are steel tubes, which are kept elastic by capacity design, having the function of extending the device into a bracing form and connecting to the main frame. The steel rods move in the slots, with the aim to elongate the SMA wires and transfer force between different members. For demonstration purpose, this brace is selected as the current bracing form, and will be equipped in the multi-story CBFs. It is seen the strength and stiffness of the adopted brace can be directly calculated by determining the cross sectional area and effective length of the NiTi SMA wires. In practical construction projects, large-diameter SMA wires or rods may be used to scale up the strength and stiffness capacity of such braces.

3. Earthquake ground motions

The structural design will be conducted at the seismic hazard level corresponding to design-basis earthquake (DBE). The considered ground motions in design procedure were generated for Los Angeles with an exceedance probability of 10% in 50 years by Somerville *et al*. (1997), whereas the seismic performance of structures are assessed by subjecting them to three seismic hazard levels, denoted as frequently-occurred earthquake (FOE), DBE and maximum-considered earthquake (MCE). A total of 60 records, designated as LA01-LA60 (LA01-LA20 for DBE, LA21-LA40 for MCE, LA41-LA60 for FOE), were derived from historical records with frequency domain adjusted and amplitude scaled. The earthquake records were modified from soil type S_B–S_C to soil type S_D. Figure 4 plots the response spectra of considered earthquake ground motions. It is seen that great variability exists among the records due to the uncertain nature of earthquakes.

4. Ductility demand and design approach

Prior to introducing the design approach for current frames, the definitions of strength reduction factor, *R*, and ductility demand, μ, are given, as defined by Chopra (2001). Fig. 5 schematically shows the force-deformation curves of inelastic system and corresponding elastic system, upon the same ground motion excitation. As shown in Fig. 5, *R* and μ are given as below

$$R = F_e / F_y \tag{1}$$

$$\mu = u_m / u_y \tag{2}$$

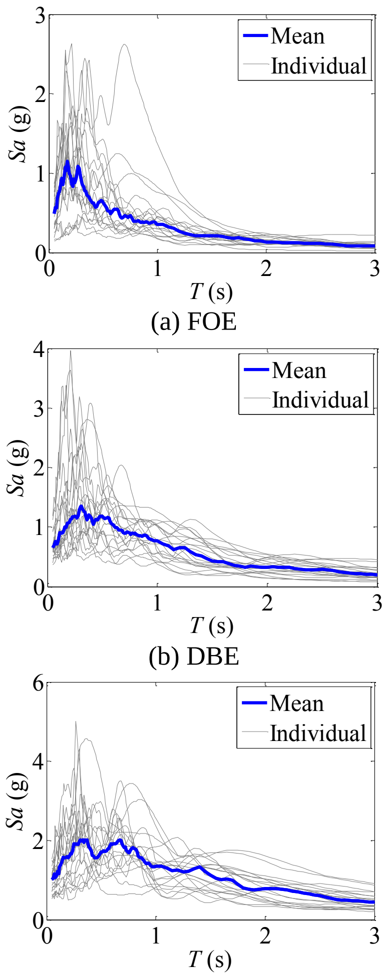

(a) FOE

(b) DBE

(c) MCE

Fig. 4 Three suites of earthquake ground motion records associated with three seismic hazard levels

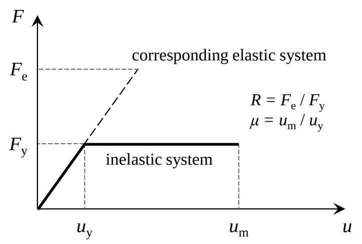

Fig. 5 Definitions of strength reduction factor, R, and ductility demand, μ

where F_e and F_y are the strength demands of elastic system and yield strength of inelastic system, respectively. u_m and u_y are the maximum deformation and yield deformation of inelastic system, respectively. It is noted again that the 'yield' behavior of SMA wire essentially refers to the forward phase transformation mechanism. Parenthetically, the magnitude of F_e not only varies with the ground motion, but also depends on the fundamental period, T. The physical meanings of R and μ indicate that an inelastic system with a lower yield strength tends to suffer from larger deformation demand.

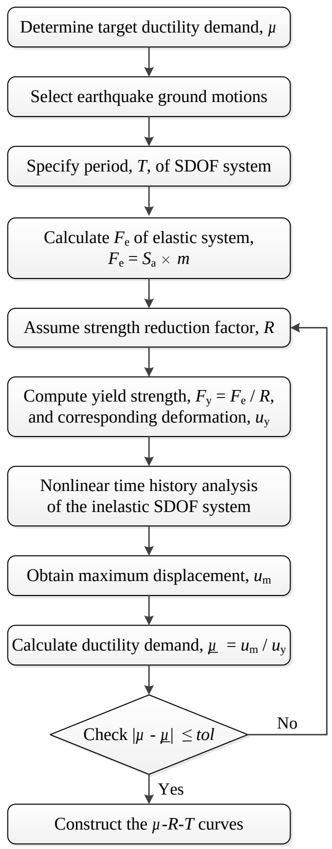

Fig. 6 Flowchart of constructing the μ-R-T curve

Fig. 6 shows the flowchart of constructing the μ-R-T curves. The target ductility demands of the single-degree-of-freedom (SDOF) systems are set to be 3, 4, 5 and 6. The upper bound of target ductility is determined to be 6, which equals to the ratio of the strain associated with the finish of forward phase transformation to that features the start of forward phase transformation. As shown in Fig. 1, the NiTi SMA wire experiences strain hardening when the ductility demand exceeds 6, which may pose excessive strength demand to the adjacent structural components of the main frame. The range of fundamental period is from 0.1 s to 3.0 s with an increment of 0.1 s, covering the vibration periods of typical braced framing structures. Iterations of the strength reduction factor are usually required until the error between the calculated ductility and prescribed ductility is within the tolerance. The tolerance for ductility demand, *tol*, is set to be 3% of the targeted ductility.

Fig. 7 presents the constant ductility demand curves of SDOF systems that representing the simplified NiTi SMA hysteresis and idealized flag-shape hysteresis. The performance of SDOF systems usually represents the global behavior of corresponding multi-degree-of-freedom (MDOF) systems. Each curve is the averaged result of 20 curves corresponding to 20 DBE ground motion records. Similar trend can be observed in each curve, which initially increases with T and tends to be stabilized in the long period range. For a specific period, large ductility demand is generated by designating large strength reduction factor,

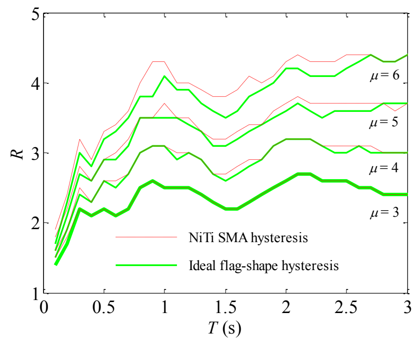

Fig. 7 Constant ductility demand curves of SDOF systems representing the hysteresis of NiTi SMA and idealized flag shape

because inelastic systems with low 'yielding' strength is prone to suffer from large deformation demand. By determining the targeted ductility and estimated period, the R value can be readily extracted from the curves. Compared with the idealized flag-shape hysteresis without the strain hardening behavior, the current hysteresis shows a similar general pattern of constant ductility demand. However, it is noted that the R values of simplified NiTi SMA hysteresis become larger than that of idealized flag-shape hysteresis, when the targeted ductility demand is increased. This comparison indicates the strain hardening behavior of NiTi SMA brings benefit of reducing the 'yield' strength capacity for such structural system.

The adopted design approach (Qiu and Zhu 2017a) directly depends on the μ-R-T relationship of the SDOF system. For concise consideration, the final expression of design base shear is given as below

$$V_y = \left(-\lambda + \sqrt{\lambda^2 + 4\gamma S_a^2}\right) \cdot W / 2 \times W \tag{3}$$

$$\gamma = \left[\alpha(\mu\text{-}1)^2 + 2\mu\text{-}1\right] / R^2 \tag{4}$$

where W is the building weight; S_a is the spectral acceleration extracted from the design spectrum given the fundamental period of the structure is known; λ is a parameter given by Eq. (18) of reference (Qiu and Zhu 2017a). The idealized flag-shape hysteresis was assumed in the development of the design method (Qiu and Zhu 2017a). Therefore, with the μ-R-T relationship for NiTi SMA hysteresis determined, the seismic design approach (Qiu and Zhu 2017a) can be directly extended to CBFs equipped with NiTi SMA braces. The key parameters of brace include the cross-section area A_i and length l_i of the SMA wires, determined as below, respectively

$$A_i = \sum_{j=i}^{n} C_j V_y / \left(2\cos\theta_i \cdot \sigma_{Ms}\right) \tag{5}$$

$$l_i = E_A \theta_y h_i \cos\theta_i / \sigma_{Ms} \tag{6}$$

where C_j is the lateral force distribution factor for multi-story CBF equipped with SMA braces; θ_i is the inclination angle of the brace in the ith story; h_i is the height of the ith story. The full design procedure is identical to that presented in reference (Qiu and Zhu 2017a).

5. Performance targets and design results

This aforementioned seismic design approach begins with setting performance targets. Considering interstory drift ratio was reported as the most straightforward damage index among various performance indices (Iwan 1997), this study selects the interstory drift ratio as the design target. To evaluate the robustness of the developed design approach, a total of four structures using different braces are designed. The design targets for all frame buildings are set to be a maximum interstory drift ratio, θ_{max}, of 1.5% upon the DBE ground motion records for all structures. It is noted that although different drift targets can be set, this study assumed a constant value in this comparative analysis and thus concentrated on the impact of hysteresis variations of bracing components. Regarding the associated ductility target of SMA braces, it varies with different frames and will be described as below. The μ values of braces directly determines the peak deformation of the NiTi SMA wire, which corresponds to the extent of forward phase transformation. Consistent with the analysis on the SDOF systems, the range of μ is also defined to be from 3 to 6 with an increment of unit. With θ_{max} and μ prescribed, the 'yield' interstory drift ratio, θ_y, and plastic interstory drift ratio, θ_p, are calculated by following equations

$$\theta_y = \theta_{\max} / \mu \tag{7}$$

$$\theta_p = \theta_{\max} - \theta_y = (\mu - 1) \times \theta_y \tag{8}$$

The fundamental period of structures can be estimated by the inelastic displacement spectrum (Priestley and Kowalsky 2000). The strength reduction factor is extracted from the constant ductility curves, since μ and T are given. The design parameters for all structures, named S1 to S4, are listed in Table 1. It is seen the fundamental period of structures decreases with the increase of ductility demand of braces, which is due to the small 'yield' interstory drift as a high ductility demand is prescribed. The strength reduction factor implies that the resulting 'yield' strength is reduced by designating high ductility to the braces. Therefore, the design outcome shows that the ductility demands and strength reduction factors are consistent with the results based on SDOF systems, as illustrated by Fig. 7.

Table 1 Design information and parameters

Parameters		S1	S2	S3	S4
T (s)	Estimation	1.26	1.16	1.09	1.06
	Result	1.29	1.21	1.16	1.13
Target μ		3	4	5	6
Target $\theta_{\max}$ (%)		1.5			
θ_y (%)		0.5	0.375	0.3	0.25
θ_p (%)		1.0	1.125	1.2	1.25
R		2.45	3.0	3.5	4.0

Table 2 Design results

Story No.		1st	2nd	3rd	4th	5th	6th
A_i	S1	2984.1	2419.5	2227.9	1944.0	1549.4	999.7
	S2	2639.3	2138.3	1966.3	1711.8	1359.1	870.5
	S3	2416.0	1956.3	1797.0	1561.7	1236.3	787.4
	S4	2206.0	1785.9	1639.8	1424.1	1126.1	715.6
l_i	S1	1.76	1.50	1.50	1.50	1.50	1.50
	S2	1.32	1.12	1.12	1.12	1.12	1.12
	S3	1.05	0.90	0.90	0.90	0.90	0.90
	S4	0.88	0.75	0.75	0.75	0.75	0.75
Beam	S1		W 14×61			W 14×48	
	S2		W 14×53			W 14×43	
	S3		W 14×48			W 14×38	
	S4		W 14×43			W 14×34	
Column	S1		W 14×159			W 14×61	
	S2		W 14×159			W 14×61	
	S3		W 14×145			W 14×53	
	S4		W 14×145			W 14×53	

Table 2 lists the design results for these CBFs. In all structures, the cross sectional area of NiTi SMA wires, A_i, at the lower stories is larger than that at the upper stories, because the lower stories sustained higher seismic forces. Comparison between S1 to S4 shows that S1 has the largest A_i at each story, for example, the A_i of S1 is approximately 30-40% larger that of S4, depending on story number. This is attributed to the fact that different strength reduction factors were used in the design procedure. For the wire length, l_i, which is found shortest in S4, because the associated θ_y was defined to be the smallest among the considered structures. The 1st-story brace has the longest length is due to that li is in a positive linear relationship with the story height, as can be seen in Eq. (6). Regarding the structural components of the main frames, i.e. the beam and column, they were sized to only sustain the axial force transferred from the SMA braces. It is worth noting that the main frame is primarily to form the truss mechanism, rather than to resist the seismic forces, since SMA braces are expected to be entirely responsible for resisting seismic forces. The sizes of sections are in the descending order from S1 to S4, which are in a negative correlation with the magnitudes of R values, because the sustained force demand is correlated to the 'yield' strength of braces.

6. Prototype multi-story CBF and numerical model

Fig. 8 shows the elevation view and plan layout of the adopted 6-story CBF, which was widely used in a number of peer work (Hou *et al.* 2017, Qiu and Zhu 2016, Qiu and Zhu 2017a, Qiu *et al.* 2017, Qiu *et al.* 2018, Sabelli *et al.* 2003). The original structure, denoted as 6vb2, was designed by Sabelli *et al.* (2003) according to NEHRP (1997) and was expected to be located in downtown Los Angeles. The chevron-braced steel frame has a bay width of 9.14 m, and its story height is 3.96 m except for the 1st story is 5.49 m. The braces are symmetrically installed at six bays in each direction, as shown in Fig. 8(a). The seismic tributary mass of each bay is 1/6 of the total floor mass. ASTM A992 steel is used for the main frame material.

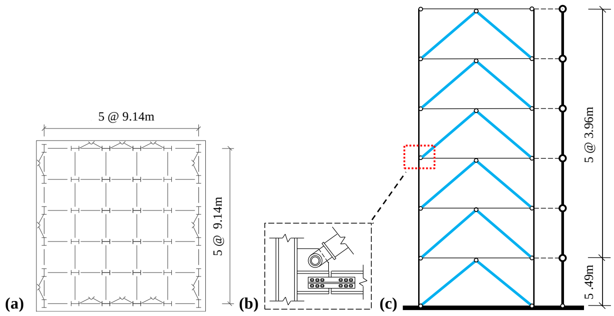

Fig. 8 Elevation view and plan layout of the 6-story CBF equipped with NiTi SMA braces

More structural details can be found in (Sabelli *et al.* 2003). All the frames are assumed to be in an indoor environment without being affected by temperature effect. Thus the SMA braces remain stable hysteresis properties and superelasticity during the following seismic analyses. Moreover, the beam-to-column connections are modified as pin connections to eliminate connection moment and accommodate large rotation without damage (Fahnestock *et al.* 2007). One viable type suggested by Fahnestock *et al.* (2007) is shown in Fig. 8(b).

Fig. 8(c) also illustrates the computer model built in OpenSees (2013). The model consists of the fixed braced frame and one leaning column, which are coupled to have equal displacements at each floor level. The adopted beam-to-column connection is achieved by coupling the displacements of two overlapped nodes while releasing their rotation constraints. For the leaning column, pins are also introduced between adjacent floors, with the purpose of inhibiting seismic resistance while generating P-Δ effect. The beams and columns are modeled with force-based beam-column elements, as suggested by previous studies (Neuenhofer and Filippou 1997). The materials of main frames and SMA braces are designated with *Steel02* and *SelfCentering*, respectively. Each member is modeled as an element whose cross section at each integration point is an assembly of uniaxial fibers. A Rayleigh damping ratio of 5% is assigned to the first two vibration modes. Sufficient time is added at the end of each earthquake ground motion, with the purposes of allowing the vibrations to damp out and accurately measuring the residual deformations.

7. Validation of the design method

This section aims to examine whether the adopted design approach produced expected results. To this end, the seismic performance of all structures are assessed upon DBE ground motions, since the design was based on this seismic hazard level. The developed seismic design approach is based on SDOF system, which usually represents the global behavior of the corresponding MDOF system. However, due to the MDOF effect, the interstory drift of a multi-story frame tends to be varied with story number and differs from the roof drift. Therefore, to have a fair assessment for the deformation demand, the mean values of the maximum interstory drift ratios among all stories upon an individual ground motion record, θ_{max}, are proposed and defined as below

$$\theta_{\max} = mean(\theta_{m,i}), \quad i = 1, \ldots, 6 \tag{9}$$

where $\theta_{m,i}$ is the maximum interstory drift ratio at the *i*th story.

The results upon ground motion records associated with DBE seismic hazard level are assembled in Table 3. Due to the uncertainty of earthquakes, significant variations can be found between the results associated with different ground motions. To understand the central tendency of the results, Table 3 also calculates the mean values of θ_{max}, which are found in the range of 1.45 to 1.52%. Compared with the design target of 1.5%, the errors between the designed results and prescribed targets are less than 3.59%. In addition, the standard deviations, *std*, are also calculated to quantitatively estimate the record-to-record variation. It can be seen the *std* is approximately 0.6 for all structures, showing that not only the mean values are very close, but also the standard deviations are nearly identical. Therefore, the examinations on θ_{max} evidently indicate the developed design approach is successfully applicable to the design of CBFs equipped with NiTi SMA braces, irrespective of how the targeted behavior of the NiTi SMA braces is prescribed at the beginning of the design.

8. Nonlinear static analysis

Nonlinear static analysis, i.e. the pushover analysis, is firstly conducted to evaluate the global seismic behavior of CBFs equipped with NiTi SMA braces. Before applying the lateral forces to the frames, gravity force was gradually loaded to the numerical model to generate the *P-Δ* effect.

The applied lateral force pattern was compliant with the first vibration mode and was maintained throughout the loading procedure. The magnitude of target displacement was set to be a roof drift of 3.0%, with a control node at the roof level.

Fig. 9 shows the monotonic loading curves for all considered structures upon the 1st-mode lateral force pattern, by plotting the relationship between the roof drift ratio and normalized base shear. It is seen that the structures 'yield' at different roof drift ratios, for example, S1 has a 'yield' roof drift ratio of approximately 0.55%, whereas S4 begins to 'yield' as the building was driven to 0.3% roof drift ratio. Compared with the design results listed in Table 1, reasonable agreements can be found. With the smallest 'yield' deformation, S3 and S4 experienced noticeable strain hardening behavior within the target displacement, because the NiTi wires of the SMA braces entirely completed the forward phase transformation. The target displacement also generated moderate strain hardening behavior in S2, whereas slight behavior in S1. This can be explained by the different targeted ductility demands of SMA braces. In addition, the normalized base shears, which is essentially the base shears normalized by the total building weight, of different structures indicate that the 'yield' strengths of resulting structures are compliant with the strength reduction factor shown in Table 1. It is interesting to note that, under moderate deformation demand, say 1.5%, S1 sustained the highest force demand, whereas S4 sustained the lowest force demand, primarily due to the strength reduction factor. Upon large deformation up to 3%, significant force demand was generated in the entire system, attributed to severe strain hardening behavior in structures of S2-S4. Therefore, it seems that the strain hardening behavior of NiTi SMAs does not necessarily produce excessive strength demand in the structures when the deformation is within design target; however, significant force will be produced by strain hardening behavior when the structures suffered excessive deformation demand.

9. Nonlinear time history analysis

The section conducted nonlinear time history analyses for the considered structures by subjecting them to the selected earthquake ground motions. Several critical seismic performance indices are assessed, with the purposes of examining the seismic performance of the CBFs equipped with different NiTi SMA braces upon multi-level seismic hazards.

9.1 Case study

In the design procedure, different ductility demands were prescribed for the SMA braces, which lead to variations of the hysteretic properties of SMA braces, as can be clearly seen in the nonlinear static analysis. This subsection is to examine how the hysteretic properties of SMA braces make influence to the seismic performance of CBFs.

Table 3 Mean values of maximum interstory drift ratios at DBE seismic hazard level (%)

Ground motions	S1	S2	S3	S4
LA1	1.42	1.47	1.47	1.49
LA2	1.42	1.33	1.22	1.20
LA3	1.01	1.06	0.94	1.13
LA4	0.72	0.67	0.68	0.66
LA5	0.93	0.86	0.95	1.18
LA6	0.47	0.46	0.47	0.49
LA7	1.10	1.13	1.10	1.07
LA8	0.93	0.96	1.06	1.11
LA9	2.56	2.39	2.20	2.08
LA10	1.56	1.49	1.48	1.46
LA11	2.38	2.31	2.11	2.06
LA12	0.88	0.86	0.84	0.82
LA13	1.67	1.60	1.62	1.67
LA14	1.95	1.82	1.73	1.74
LA15	1.88	1.79	1.79	1.77
LA16	2.30	2.24	2.23	2.17
LA17	1.40	1.41	1.34	1.57
LA18	2.62	2.56	2.46	2.35
LA19	1.11	1.13	1.26	1.25
LA20	2.12	2.04	1.95	2.02
Statistical measure				
mean	1.52	1.48	1.45	1.46
error	1.50	-1.37	-3.59	-2.38
std	0.64	0.61	0.56	0.52

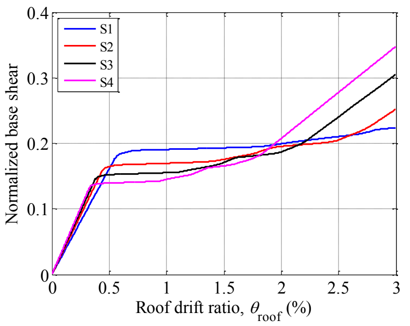

Fig. 9 Monotonic loading curves of various frames upon the 1st-mode lateral force pattern

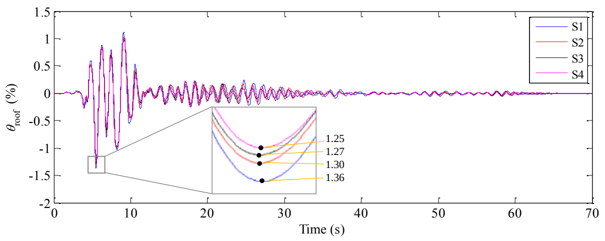

(a) roof drift time history

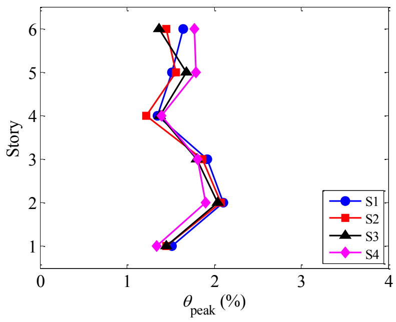

(b) peak interstory drift ratios along building height

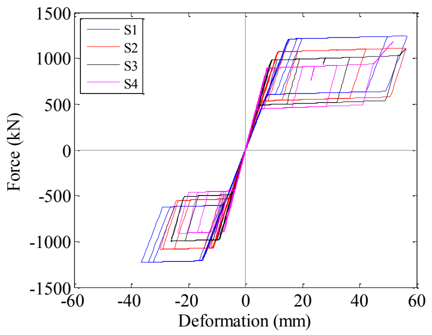

(c) force-deformation relationships of the 2nd-story braces

Fig. 10 Effect of hysteretic properties of NiTi SMA braces upon record LA13

It is worth noting that the selected case does not necessarily assure the individual case will accurately match the prescribed target, since the design approach is oriented from the statistical analyses on SDOF systems under twenty ground motion records. A representative ground motion record associated with DBE seismic hazard level, LA13, was selected for demonstration purpose, because the corresponding spectral accelerations well coincide with the design spectrum in the period range covering the fundamental periods of the considered structures.

Fig. 10(a) compares the roof drift time histories with the peaks marked. It is seen the roofs vibrate with an approximately identical frequency and amplitude throughout the entire time duration and come to rest with zero residual deformation at the end of earthquake. The peaks of S1 to S4 are marked as 1.36, 1.30, 1.27 and 1.25%, respectively, indicating a small difference corresponding to less than 10%. Fig. 10(b) presents the peak interstory drift ratios along building height, showing the behaviors are comparable in every single story and the maximum demand tends to occur at the second story upon the selected ground motion. The assessment of deformation demands illustrates that the CBFs are able to exhibit comparable performance, although they are equipped with different SMA braces.

Fig. 10(c) plots the force-deformation relationships of the second-story braces for demonstration purpose, because they sustained the largest deformations. It is interesting to note that the highest force demand was generated in the brace belonged to S1, while remarkable strain hardening behavior was actually activated in that belonged to S4. This can be understood by reading Table 1, which illustrates the high strength reduction factor well capped the maximum force demand in the main frame system. The hysteresis performance of SMA braces in this time history analysis also indicates the potential over strength effect induced by the strain hardening behavior of NiTi SMAs can be well controlled by the current design approach.

9.2 Peak interstory drift ratio

For multi-story frames, their seismic responses are prone to be affected by the story-to-story deviation. In this regard, the central tendency of the peak interstory drift ratios at each story needs assessment. Thus the averaged peak interstory drift ratios, θ_{peak}, at each story is calculated as below

$$\theta_{peak} = mean(\theta_{p,j}) , \quad j = 1, \ldots, 20 \tag{10}$$

where $\theta_{p,j}$ is the peak interstory drift ratio upon the jth ground motion record for each story. Figure 11 assembles the θ_{peak} along building height for all structures. At each hazard level, it is seen that all the structures show desirable drift performance and exhibit a uniform distribution of deformation over building height. The smaller deformation demand at the bottom story is primarily due to the contribution of the fixed column bases in resisting the seismic forces. Particularly, at the FOE level, the structural behaviors are dominant by their elastic properties, and the performance difference arises from the fundamental periods; at the DBE level, the performance target of 1.5% is plotted for examination purpose, indicating the designed structures successfully meet targets very well; at the MCE level, S1 exhibited larger deformation than the counterparts to a certain degree, because the strain hardening behavior in the other three structures is well activated and helpful to control deformation demand.

Therefore, the CBFs generally exhibit comparable deformation behaviors in each single story regardless of brace properties, as long as these braces were properly designed. The strain hardening behavior of NiTi SMA is found beneficial to control peak deformation demand.

9.3 Ductility demand of SMA braces

The SMA braces, as the core component in the seismically resistant system, are examined in terms of ductility demands. Fig. 12 assembles the maximum ductility demands of braces among all stories in total seismic analysis cases as a function of peak ground acceleration (PGA). Each dot represents the maximum ductility among six braces in each structure upon a single earthquake scenario.

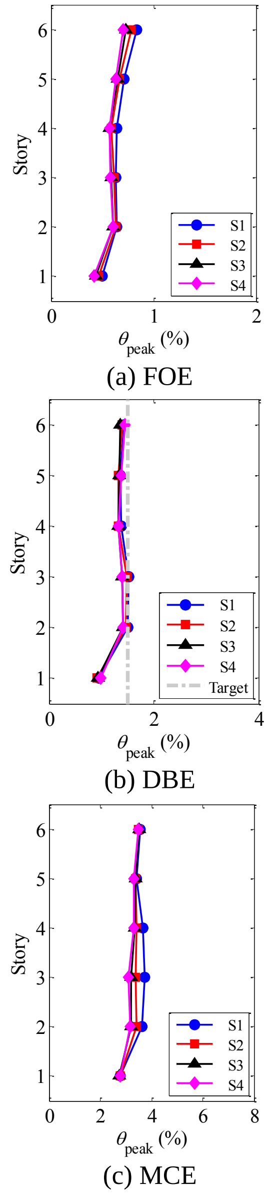

Fig. 11 Mean values of peak interstory drift ratios along building height

As prescribed, the braces sustained different ductility demands, although the structures experienced similar displacements. The strain hardening behavior of SMA braces in CBFs occurred to different extents, depending on the prescribed ductility targets. As well shown is the fitting curve, which adopts the assumption that the performance index and the logarithm of PGA have a positive linear relationship (Cornell *et al.* 2000). The fitting equations of μ and PGA for structures S1-S4 are given as below

$$\mu = \begin{cases} 7.61 \times PGA^{1.01} & S1 \\ 9.23 \times PGA^{0.98} & S2 \\ 10.66 \times PGA^{0.93} & S3 \\ 11.98 \times PGA^{0.9} & S4 \end{cases} \tag{11}$$

where PGA has the unit of *g*, which is the acceleration of gravity. Fig. 12(e) collects all the fitting curves and clearly shows that the larger the ductility target is set, the more severe the braces endured strain hardening.

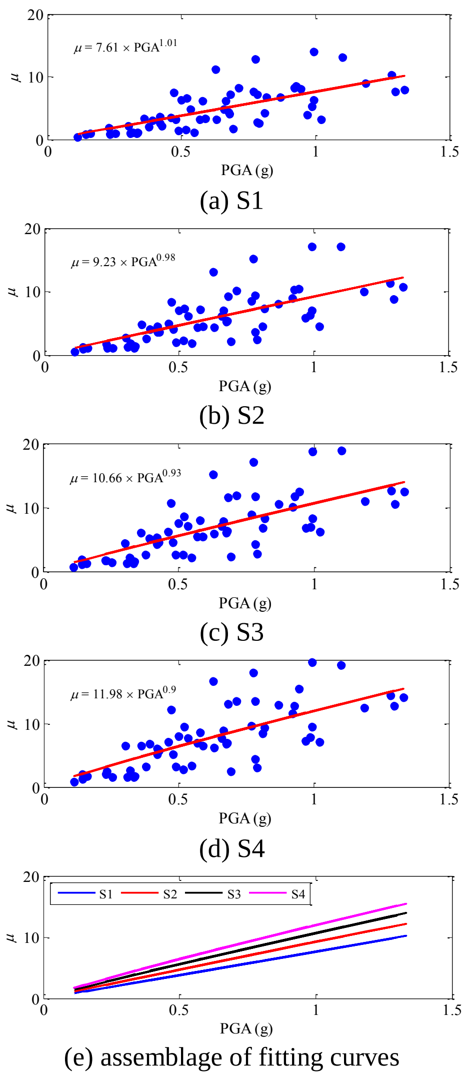

Fig. 12 Discrete data and associated fitting curves for the maximum ductility demands of NiTi SMA braces upon three suites of ground motion records

9.4 Residual interstory drift ratio

Fig. 13 presents the mean values of residual interstory drift ratio over building height. At both FOE and DBE seismic hazard levels, regardless of structural properties, all responses are nearly zero, indicating the residual deformations after earthquakes were completely eliminated by installing the SMA braces.

Although the design procedure did not explicitly take into account the residual deformation, the results show that the designed structures well produced the excellent recentering capability which is offered by the NiTi SMA wires. As aforementioned, upon those devastating earthquakes, some braces may undergo severe strain hardening behavior, leading to excessive force demand on the adjacent components of the main frame.

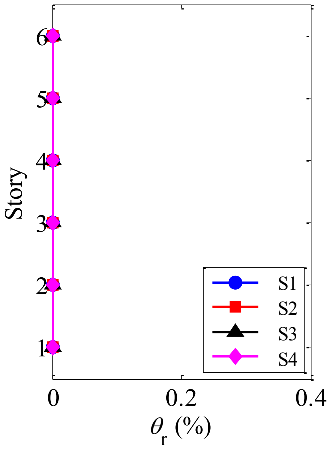

(a) FOE

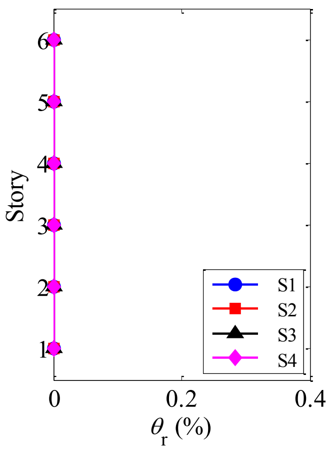

(b) DBE

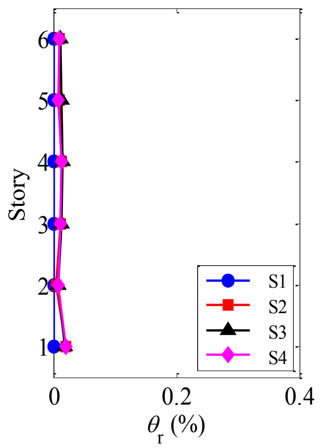

(c) MCE

Fig. 13 Mean values of residual interstory drift ratios along building height

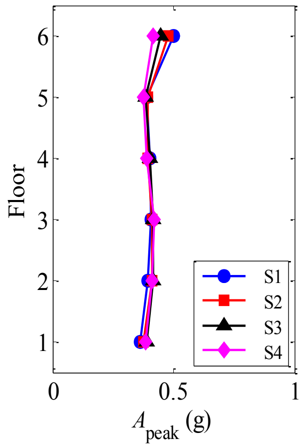

(a) FOE

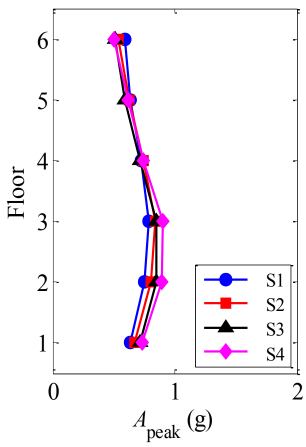

(b) DBE

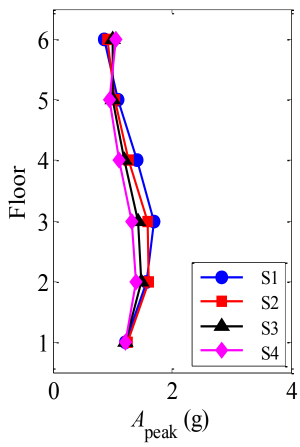

(c) MCE

Fig. 14 Mean values of peak floor accelerations along building height

Fig. 13(c) shows the residual deformation is not completely eliminated at the MCE seismic hazard level. However, the residual deformation is still very small and the structures are able to stand upright, which indicates the well designed CBFs maintain recentering capability, even though strain hardening behavior is severely produced in the braces.

9.5 Peak floor acceleration

Floor accelerations are usually deemed to be closely related to seismic damages of nonstructural components. Thus, besides with deformations, floor accelerations are also assessed, although this index was not included in the design procedure. Fig. 14 assembles the mean values of peak floor accelerations over building height, and shows the results are less than 0.5, 1.0 and 2.0 g upon FOE, DBE and MCE seismic hazard levels, respectively. According to the suggestions by (Qiu and Zhu 2017a), the acceleration demands of the designed structures are within allowable limitations. Compared with peak deformations, floor accelerations show a relatively biased distribution. The maximum accelerations are amplified at the roof at the FOE level and tend to concentrate at the second and third floors at the DBE and MCE levels. In terms of the comparisons among these structures, it is interesting to note that the acceleration demands do not show a clear relationship with the prescribed ductility demands.

10. Conclusions

This study aims to examine the seismic performance of properly designed CBFs equipped with NiTi SMA braces. The current CBFs were designed by an *ad hoc* seismic design approach (Qiu and Zhu 2017a). The constant ductility demand curves for the SDOF systems representing the hysteresis of NiTi SMAs are established. Particularly, the strain hardening behavior upon large strain amplitude is well simulated and taken into account in the design procedure. A total of four different ductility demand targets were prescribed for the SMA braces, while the associated structures were set with the same drift target. The designed structures were subjected to three suites of ground motion records corresponding to three seismic hazard levels, and the following conclusions can be obtained:

- The constant ductility demands of NiTi SMA-based SDOF systems shows a similar pattern as that of the idealized flag-shape hysteresis without the strain hardening behavior.
- Setting a low ductility demand target for NiTi SMA braces generally avoids activating the strain hardening behavior, whereas setting a high ductility target well reduces the 'yield' strength for the structural system.
- Although a variety of ductility demands were prescribed for the braces in different CBFs, all the structures met an identical drift target.
- Regardless of how the NiTi SMA braces performed, the associated structures exhibited uniform deformation demands over building height, eliminated residual deformation and controllable acceleration demands.
- The strain hardening behavior of NiTi SMA wires is beneficial to control deformations, whereas does not deteriorate recentering capability or produce excessive floor accelerations.

Although numerical simulations well discussed the seismic behavior of CBFs equipped with NiTi SMA braces, experimental tests for reduced- or real- scale building models are needed to be carried out in future, with the aim to validate the conclusions by providing solid experimental data. To demonstrate the seismic behavior of properly designed CBFs equipped with NiTi SMA braces, this study selected one viable configuration for the braces. The current study is a general analysis on such frame buildings, and the obtained conclusions also shed light on those frames using different SMA braces.

Acknowledgements

This research was supported by the financial support from the China Postdoctoral Science Foundation (No.: 2017M622206), the Natural Science Foundation of Shandong Province, China (No.: ZR2017BEE004), the Fundamental Research Funds of Shandong University (No.: 2016HW011), the Open Fund of the National Engineering Technology and Research Center for Prefabrication Constructions in Civil Engineering and the Special Fund of Prof. Zuyan Shen (No.: 2014CPCCE-K03). The authors wish to acknowledge the sponsors. However, any opinions, findings, conclusions and recommendations presented in this paper are those of the authors and do not necessarily reflect the views of the sponsors.

References

Abou-Elfath, H. (2017), “Evaluating the ductility characteristics of self-centering buckling-restrained shape memory alloy braces”, *Smart Mater. Struct.*, **26**(5), 055020.

Andrawes, B. and DesRoches, R. (2005), “Unseating prevention for multiple frame bridges using superelastic devices”, *Smart Mater. Struct.*, **14**(3), 60-67.

Andrawes, B. and DesRoches, R. (2008). “Sensitivity of seismic applications to different shape memory alloy models”. *J. Eng. Mech.*, **134**(2), 173-183.

Araki, Y., Endo, T., Omori, T., Sutou, Y., Koetaka, Y., Kainuma, R. and Ishida, K. (2011), “Potential of superelastic Cu–Al–Mn alloy bars for seismic applications”, *Earthq. Eng. Struct. D.*, **40**(1), 107-115.

Carreras, G., Casciati, F., Casciati, S., Isalgue, A., Marzi, A. and Torra, V. (2011), “Fatigue laboratory tests toward the design of SMA portico-braces”, *Smart Struct. Syst.*, **7**(1), 41-57.

Casciati, F. and Faravelli, L. (2009), “A passive control device with SMA components from the prototype to the model”, *Struct. Control. Health. Monit*, **16**(7-8), 751-765.

Casciati, S., Faravelli, L. and Vece, M. (2017), “Investigation on the fatigue performance of Ni-Ti thin wires”, *Struct. Control Health Monit.*, **24**, e1855. doi: 10.1002/stc.1855.

Casciati, S. and Marzi, A. (2010), “Experimental studies on the fatigue life of shape memory alloy bars”, *Smart Struct. Syst.*, **6**(1), 73-85.

Casciati, S. and Marzi, A. (2011), “Fatigue tests on SMA bars in span control", *Eng. Struct.*, **33**(33), 1232-1239.

Chopra, A.K. (2001), *Dynamics of structures theory and applications to earthquake engineering*, Upper Saddle River NJ Prentice-Hall.

Cornell, A.C., Jalayer, F. and Hamburger, R.O. (2002), "Probabilistic basis for 2000 SAC federal emergency management agency steel moment frame guidelines", *J. Struct. Eng.- ASCE*, **128**, 526-532.

DesRoches, R., McCormick, J. and Delemont, M. (2004), "Cyclic properties of superelastic shape memory alloy wires and bars", *J. Struct. Eng. - ASCE*, **130**(1), 38-46.

DesRoches, R. and Smith, B. (2004), "Shape memory alloys in seismic resistant design and retrofit: a critical review of their potential and limitations", *J. Earthq. Eng.*, **8**(3), 415-429.

Dezfuli, F.H. and Alam, M.S. (2013), "Shape memory alloy wire-based smart natural rubber bearing", *Smart Mater. Struct.*, **22**(4), 045013.

Dolce, M., Cardone, D. and Marnetto, R. (2000), "Implementation and testing of passive control devices based on shape memory alloys", *Earthq. Eng. Struct. D.*, **29**(7), 945-968.

Dolce M, Cardone, D, Ponzo FC and Valente C (2010), "Shaking table tests on reinforced concrete frames without and with passive control systems", *Earthq. Eng. Struct. D.*, **34**(14), 1687-1717.

Fahnestock, L.A., Ricles, J.M. and Sause, R. (2007), "Experimental evaluation of a large-scale buckling-restrained braced frame", *J. Struct. Eng.- ASCE*, **133**(9), 1205-1214.

Fang, C., Wang, W., He, C. and Chen, Y.Y. (2017), "Self-centring behaviour of steel and steel-concrete composite connections equipped with NiTi SMA bolts", *Eng. Struct.* **150**, 390-408.

Fang, C., Yam, M.C.H., Lam, A.C.C. and Xie, L.K. (2014), "Cyclic performance of extended end-plate connections equipped with shape memory alloy bolts", *J. Constr. Steel. Res.*, **94**, 122-136.

FEMA 1997 NEHRP Recommended provisions for seismic regulations for new buildings and other structures, Federal Emergency Management Agency Washington DC.

Gao, N., Jeon, J.S., Hodgson, D.E. and DesRoches, R. (2016), "An innovative seismic bracing system based on a superelastic shape memory alloy ring", *Smart Mater. Struct.*, **25**(5), 055030.

Hadi, A. and Akbari, H. (2016), "Modeling and control of a flexible continuum module actuated by embedded shape memory alloys. ", *Smart Mater. Struct.*, **18**(4), 663-682.

Hou, H.T., Li, H., Qiu, C.X. and Zhang, Y.C. (2017). "Effect of hysteretic properties of SMAs on seismic behavior of self-centering concentrically braced frames". *Struct. Control Health. Monit.*, DOI: 10.1002/stc.2110.

Iwan, W.D. (1997), "Drift spectrum measure of demand for earthquake ground motions", *J. Struct. Eng.-ASCE*, **123**(4) 397-404.

Katariya P.V., Panda, S.K., Hirwani C.K., Mehar K. and Thakare O. (2017), "Enhancement of thermal buckling strength of laminated sandwich composite panel structure embedded with shape memory alloy fibre", *Smart Struct. Syst.*, **20**(5), 595-605.

Liu, J.L., Zhu, S., Xu, Y.L. and Zhang, Y.F. (2011), "Displacement-based design approach for highway bridges with SMA isolators", *Smart Struct. Syst.*, **8**(2), 173-190.

McCormick, J., DesRoches, R., Fugazza, D. and Auricchio, F. (2007), "Seismic assessment of concentrically braced frames with shape memory alloy braces", *J. Struct. Eng. -ASCE*, **133**(6), 862-870.

Moradi, S., Alam, M.S. and Asgarian, B. (2014), "Incremental dynamic analysis of steel frames equipped with NiTi shape memory alloy braces", *Struct. Des. Tall Spec. Build.*, **23**(18), 1406-1425.

Neuenhofer, A. and Filippou, F.C. (1997), "Evaluation of nonlinear frame finite-element models", *J. Struct. Eng.- ASCE*, **123**(7), 958-966.

OpenSees (2013), "Open system for earthquake engineering simulation (OpenSees) [Computer software]", Pacific Earthquake Engineering Research Center Berkeley CA.

Ozbulut, O.E., Hurlebaus, S. and Desroches, R. (2011), "Seismic response control using shape memory alloys a review", *J. Intel. Mat. Syst. Str.*, **22**(14), 1531-1549.

Ozbulut, O.E. and Silwal B. (2016), "Performance assessment of buildings isolated with S-FBI system under near-fault earthquakes", *Smart Struct. Syst.*, **17**(5), 709-724.

Park J.K. and Park S. (2016), "Intelligent bolt-jointed system integrating piezoelectric sensors with shape memory alloys", *Smart Struct. Syst.*, **17**(1), 135-147.

Priestley, M.J.N. and Kowalsky, M.J. (2000), "Direct displacement-based seismic design of concrete buildings", *B. N.Z. Soc. Earthq. E.*, **33**(4) 421-444.

Qian, H., Li, H. and Song, G. (2016), "Experimental investigations of building structure with a superelastic shape memory alloy friction damper subject to seismic loads", *Smart Mater. Struct.*, **25**(12), 125026.

Qiu, C. and Zhu, S. (2016), "High-mode effects on seismic performance of multi-story self-centering braced steel frames", *J. Constr. Steel Res.*, **119**, 133-143.

Qiu, C. and Zhu, S. (2017a), "Performance-based seismic design of self-centering steel frames with SMA-based braces", *Eng. Struct.*, **130**, 67-82.

Qiu, C. and Zhu, S. (2017b), "Shake table test and numerical study of self-centering steel frame with SMA braces", *Earthq. Eng. Struct. D.*, **46**, 117-137.

Qiu, C. and Zhu, S. (2014), "Characterization of cyclic properties of superelastic monocrystalline Cu–Al–Be SMA wires for seismic applications", *Constr. Build. Mater.*, **72**, 219-230.

Qiu, C., Li, H., Ji, K.F., Hou, H.T. and Tian, L. (2017), "Performance-based plastic design approach for multi-story self-centering concentrically braced frames using SMA braces", *Eng. Struct.*, **153**, 628-638.

Qiu, C., Zhang, Y.C., Li, H., Qu, B., Hou, H.T., and Tian, L. (2018), "Seismic performance of concentrically braced frames with non-buckling braces: a comparative study". *Eng. Struct.*, **154**, 93-102.

Sabelli, R., Mahin, S. and Chang, C. (2003), "Seismic demands on steel braced frame buildings with buckling-restrained braces", *Eng. Struct.*, **25**(5), 655-666.

Shrestha, B. and Hao, H. (2016), "Parametric study of seismic performance of super-elastic shape memory alloy-reinforced bridge piers", *Struct. Infrastruct. Eng.*, **12**(9), 1076-1089.

Sommerville, P.G., Smith, N.F., Punyamuthula, S. and Sun, J. (1997), Development of ground motion time histories for Phase 2 of the FEAM/SAC steel project SAC *Background Document SAC/BD-91/04 SAC Joint Venture Sacramento Calif*.

Song, G., Ma, N. and Li, H.N. (2006), "Applications of shape memory alloys in civil structures", *Eng. Struct.*, **28**(9), 1266-1274.

Torra, V., Carreras, G., Casciati, S. and Terriault, P. (2014), "On the NiTi wires in dampers for stayed cables", *Smart Struct. Syst.*, **13**(3), 353-374.

Torra, V., Martorell, F., Lovey F.C. and Sade, M.L. (2017), "Civil Engineering Applications: Specific Properties of NiTi Thick Wires and Their Damping Capabilities, A Review", *Shap. Mem. Superelasticity*, **3**:403-413.

Uang, C.M., Bruneau, M., Whittaker, A.S. and Tsai, K.C. (2001), *Seismic Design of Steel Structures The Seismic Design Handbook*",Springer ,US.

Zhang, Y. and Zhu, S. (2007), "A shape memory alloy-based reusable hysteretic damper for seismic hazard mitigation", *Smart Mater. Struct.*, **16**(5), 1603.

Zhang, Y., Hu, X. and Zhu, S. (2010), "Seismic performance of

benchmark base-isolated bridges with superelastic Cu–Al–Be restraining damping device", *Struct. Control. Health. Monit.*, **16**(6), 668-685.
Zhu, S. and Zhang, Y. (2008), "Seismic analysis of concentrically braced frame systems with self-centering friction damping braces", *J. Struct. Eng. - ASCE*, **134**(1), 121-131.

FC